ELSEVIER

Engineering Geology 58 (2000) 251–270

ENGINEERING GEOLOGY

www.elsevier.nl/locate/enggeo

A seismic landslide susceptibility rating of geologic units based on analysis of characteristics of landslides triggered by the 17 January, 1994 Northridge, California earthquake

Mario Parise [a,*], Randall W. Jibson [b]

[a] *National Research Council, Centro di Studio sulle Risorse Idriche e la Salvaguardia del Territorio, Via Orabona 4, 70125 Bari, Italy*
[b] *US Geological Survey, Box 25046, MS 966, Denver Federal Center, Denver, CO 80225, USA*

Received 2 November 1998; accepted for publication 7 January 2000

Abstract

One of the most significant effects of the 17 January, 1994 Northridge, California earthquake ($M=6.7$) was the triggering of thousands of landslides over a broad area. Some of these landslides damaged and destroyed homes and other structures, blocked roads, disrupted pipelines, and caused other serious damage. Analysis of the distribution and characteristics of these landslides is important in understanding what areas may be susceptible to landsliding in future earthquakes. We analyzed the frequency, distribution, and geometries of triggered landslides in the Santa Susana 7.5′ quadrangle, an area of intense seismic landslide activity near the earthquake epicenter. Landslides occurred primarily in young (Late Miocene through Pleistocene) uncemented or very weakly cemented sediment that has been repeatedly folded, faulted, and uplifted in the past 1.5 million years. The most common types of landslide triggered by the earthquake were highly disrupted, shallow falls and slides of rock and debris. Far less numerous were deeper, more coherent slumps and block slides, primarily occurring in more cohesive or competent materials. The landslides in the Santa Susana quadrangle were divided into two samples: single landslides (1502) and landslide complexes (60), which involved multiple coalescing failures of surficial material. We described landslide morphologies by computing simple morphometric parameters (area, length, width, aspect ratio, slope angle). To quantify and rank the relative susceptibility of each geologic unit to seismic landsliding, we calculated two indices: (1) the susceptibility index, which is the ratio (given as a percentage) of the area covered by landslide sources within a geologic unit to the total outcrop area of that unit; and (2) the frequency index [given in landslides per square kilometer (ls/km^2)], which is the total number of landslides within each geologic unit divided by the outcrop area of that unit. Susceptibility categories include very high ($>2.5\%$ landslide area or >30 ls/km^2), high (1.0–2.5% landslide area or 10–30 ls/km^2), moderate (0.5–1.0% landslide area or 3–10 ls/km^2), and low ($<0.5\%$ landslide area and <3 ls/km^2).

Keywords: California; Earthquake; Landslide susceptibility; Northridge; Seismically induced landslide

* Corresponding author. Fax: +39-080-556-7944.
E-mail addresses: cerimp06@area.ba.cnr.it (Mario Parise), jibson@usgs.gov (R.W. Jibson)

0013-7952/00/$ - see front matter
PII: S0013-7952(00)00038-7

1. Introduction

Landslides have been one of the major causes of damage and casualties in many recent earthquakes (Kobayashi, 1981; Keefer, 1984; Plafker and Galloway, 1989; Schuster, 1996). Although many studies have involved extensive documentation concerning the identification and description of landslides in particular earthquakes (i.e. Cotecchia, 1986; Jibson et al., 1994a), far less work has been devoted to the assessment of the future hazards related to seismically induced landslides.

The 1994 Northridge, California earthquake is the first earthquake to produce all of the data sets needed to conduct a detailed analysis of the factors related to the seismic triggering of landslides (Jibson et al., 1998; this volume). In this paper, we analyze the frequency, distribution, and geometries of triggered landslides in the Santa Susana quadrangle, an area of intense seismic landslide activity near the earthquake epicenter. To provide context, we briefly describe the Northridge earthquake and its setting, give an overview of landslides triggered by the earthquake, and describe the geology and physiography of the Santa Susana quadrangle. We then present some simple statistical measures of landslide morphology and compare them for landslides in various geologic units. Finally, we analyze landslide distribution and frequency by geologic unit and quantify measures of relative susceptibility to seismic landsliding for each unit.

2. The Northridge earthquake and its setting

The 17 January, 1994 Northridge, California earthquake ($M=6.7$) caused widespread damage and huge economic losses. The earthquake struck the San Fernando Valley, about 30 km northwest of Los Angeles (Fig. 1) at 4:31 a.m. Pacific standard time. Though of moderate magnitude, this was the most costly earthquake in US history, with losses estimated at more than $30 billion. The earthquake occurred on a blind thrust fault (strike N70–80°W, dip 35–40°S) at a depth of about 19 km; the rupture began at the southeastern corner of the slip area and propagated upward and northwestward (Wald et al., 1994, 1996). One of the most significant geologic effects of the earthquake was the triggering of thousands of landslides over a broad area (Harp and Jibson, 1995, 1996). Some of these landslides damaged and destroyed homes and other structures, blocked roads, disrupted pipelines, and caused other serious damage.

The San Fernando Valley and the adjacent mountains are part of the Transverse Ranges physiographic province, one of the most seismically active parts of the United States. Since 1970, three damaging earthquakes have occurred in this area: the 1971 San Fernando ($M=6.6$), the 1987 Whittier Narrows ($M=5.9$), and the 1994 Northridge ($M=6.7$) earthquakes. Although similar in magnitude to the 1994 Northridge earthquake, the 1971 San Fernando earthquake caused much less damage because it struck the sparsely populated San Gabriel Mountains, whereas the Northridge earthquake was centered directly beneath the heavily populated San Fernando Valley (Hauksson and Jones, 1994); moreover, extensive growth and development since 1971 increased the risk exposure in the area.

The Northridge earthquake produced one of the most comprehensive data sets to date. About 200 strong-motion recordings of the mainshock were written, and comprehensive documentations of geologic effects, including landslides, have been completed and published [see, for example, papers in a special issue of the Bulletin of the Seismological Society of America (Teng and Aki, 1996), and in several publications by the US Geological Survey (1994, 1996)].

3. Landslides triggered by the earthquake

The Northridge earthquake triggered more than 11,000 landslides over an area of about 10,000 km^2 (Harp and Jibson, 1995, 1996) in a pattern that is roughly concentric about the epicenter (Fig. 1). The maximum distance of landslides from the Northridge epicenter is about 70 km. This broad area of widely scattered landslide activity encloses a smaller area of about 1000 km^2 of much more concentrated landsliding north and

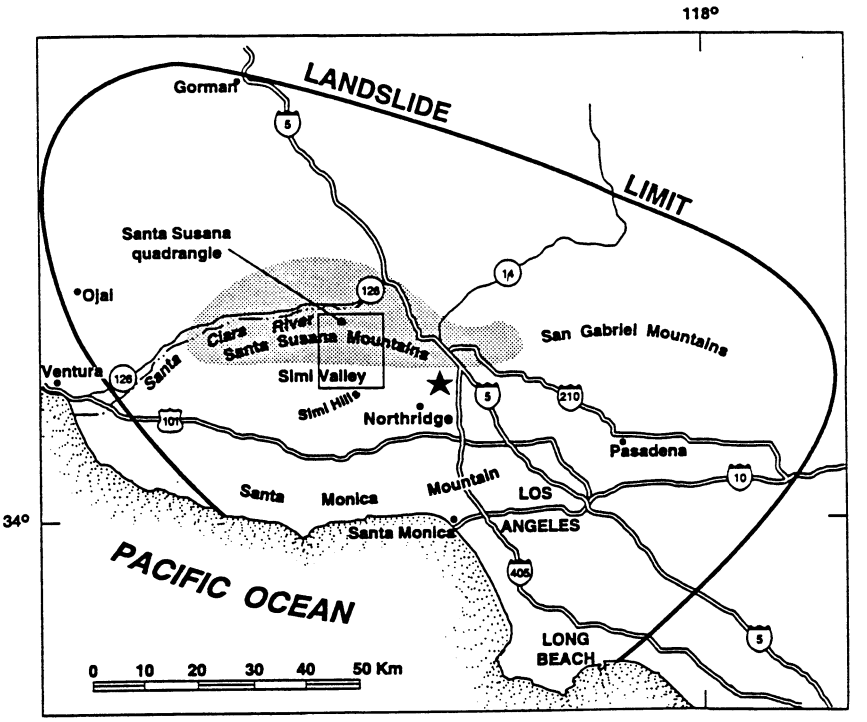

Fig. 1. Map showing epicenter of Northridge earthquake (star), limit of landslides triggered by the earthquake (solid line), area of greatest landslide concentration (shaded), and location of the Santa Susana quadrangle (box).

northwest of the epicenter. This area of high landslide concentration, which is generally less than 30 km from the epicenter, includes the Santa Susana Mountains and the mountains north of the Santa Clara River valley (see Fig. 1). This is also the area where the largest permanent ground deformations were observed: Global Positioning System (GPS) measurements of regional ground deformation collected in the weeks following the earthquake showed that horizontal displacements of nearly 20 cm and vertical displacements greater than 40 cm occurred north of the mainshock in the Santa Susana Mountains (Shen et al., 1996; Wald et al., 1996).

In the area of greatest concentration, landslides occurred in young (Late Miocene through Pleistocene) uncemented or very weakly cemented sediment that has been repeatedly folded, faulted, and uplifted in the past 1.5 million years, signifying a very rapid deformation rate. The combination of low material strength and relatively rapid uplift creates steep, unstable slopes that are highly susceptible to failure during earthquakes (Jibson et al., 1994b).

Harp and Jibson (1995, 1996) mapped landslides triggered by the Northridge earthquake from airphotos taken about 6 h after the earthquake by the US Air Force (nominal scale 1:60,000). Landslide perimeters were then digitized in the Arc/Info Geographic Information System (GIS) for plotting and analysis.

By far the most common types of landslide triggered by the earthquake, numbering in the thousands, were highly disrupted, relatively shallow (1–2 m deep, on average) falls and slides of rock and debris. Far less numerous (tens to perhaps hundreds) were deeper (10–50 m deep), more coherent slumps and block slides; these slides occurred primarily in somewhat more cohesive or competent materials (Harp and Jibson, 1995).

One notable liquefaction-induced landslide was triggered by the Northridge earthquake in the

Santa Susana quadrangle. The slide occurred in Tapo Canyon, north of Simi Valley, in artificial fill in a quarry. Strong shaking caused liquefaction of an embankment tailings dam, and a flow slide of tailings through a breach in the dam resulted (Stewart et al., 1995, 1996). The extent of the failure affected an area greater than 75,000 m^2. Being the only recognized liquefaction-induced slope movement in the Santa Susana quadrangle, the failure at Tapo Canyon will not be considered in the morphometric and statistical analyses in this paper.

4. The Santa Susana quadrangle

We analyzed the landslides triggered in the Santa Susana 7.5′ quadrangle (Fig. 1). We chose the Santa Susana quadrangle for several reasons: (1) during the Northridge earthquake, this quadrangle experienced some of the most intense landsliding in the epicentral region; (2) the quadrangle lies close to the 1994 epicenter and fault-rupture surface and experienced high levels of ground shaking; (3) almost all of the representative geologic units in the region are present in the quadrangle; (4) topography in the quadrangle ranges from flat alluvial valleys through gently sloping foothills to extremely steep canyons.

The physiography of the area resembles that of the rest of the Transverse Ranges: parallel, east–west trending mountain ranges and intervening, sediment-filled valleys. The most prominent feature in the Santa Susana quadrangle is the E–W and ESE–WNW orientation of its elongate mountains and valleys (Fig. 2). The young, weakly cemented to uncemented sedimentary rocks have been uplifted and deformed by recent tectonic activity. These weak materials erode readily and have formed deeply incised valleys separated by steep-sided ridges culminating in sharp divides.

Primary drainages in the quadrangle include the Arroyo Simi and its right tributary, Tapo Canyon (with its tributaries Tripas, Gillibrand, and Windmill Canyons), which flow down Oak Ridge and the Santa Susana Mountains. These drainages are aligned north–south to north–northeast–south–southwest for most of their courses. Elevations in the quadrangle range from about 270 m in the Simi Valley up to about 950 m in the Santa Susana Mountains (Fig. 2).

The major areas having steep slopes include the Santa Susana Mountains in the northern and northeastern parts of the quadrangle, Oak Ridge in the northwestern corner, and the foothills of the Simi Hills in the southern and southeastern parts of the quadrangle. The broad, nearly flat Simi Valley lies between the Santa Susana Mountains and Simi Hills.

Table 1 lists the geologic units cropping out in the Santa Susana quadrangle, and provides a brief description of their lithologies. Fig. 3 shows the distribution of the geologic units and indicates their exposure areas and the relative proportion of the quadrangle each unit covers. Holocene alluvium (Qal), which in general is exposed in relatively flat-lying areas not susceptible to landslides, covers 22% of the study area. Among the geologic units in sloping areas, the Chatsworth and Modelo Formations have the greatest exposure: each covers about 13% of the quadrangle. Each of the other formations covers less than 10% of the study area.

Three geologically distinct areas can be identified in the Santa Susana quadrangle: (1) the prominent mountain ridges (Santa Susana Mountains, Oak Ridge, Big Mountain) in the northern half of the quadrangle, which consist primarily of Neogene and Pleistocene sediments; (2) the Simi Valley, consisting primarily of Quaternary alluvium, in the south–central and southwestern parts of the quadrangle; and (3) the Simi Hills, consisting of Upper Cretaceous and Lower Tertiary rocks, in the southern and southeastern part of the quadrangle.

The Santa Susana Mountains are composed of uncemented or weakly cemented sandstone, siltstone, and shale. As noted previously, these mountains are being uplifted rapidly and form very steep slopes. Ridges extend primarily in northwest–southeast trending bands that parallel the axes of the main faults and folds in the area. Strata generally dip northeastward or southwestward. Principal formations include: (1) the Miocene Modelo Formation, consisting primarily of shale with some sandy units; (2) the Pliocene Towsley and Pico Formations, consisting of sandstone and siltstone; and (3) the Pleistocene Saugus Formation, consisting of sandstone with some

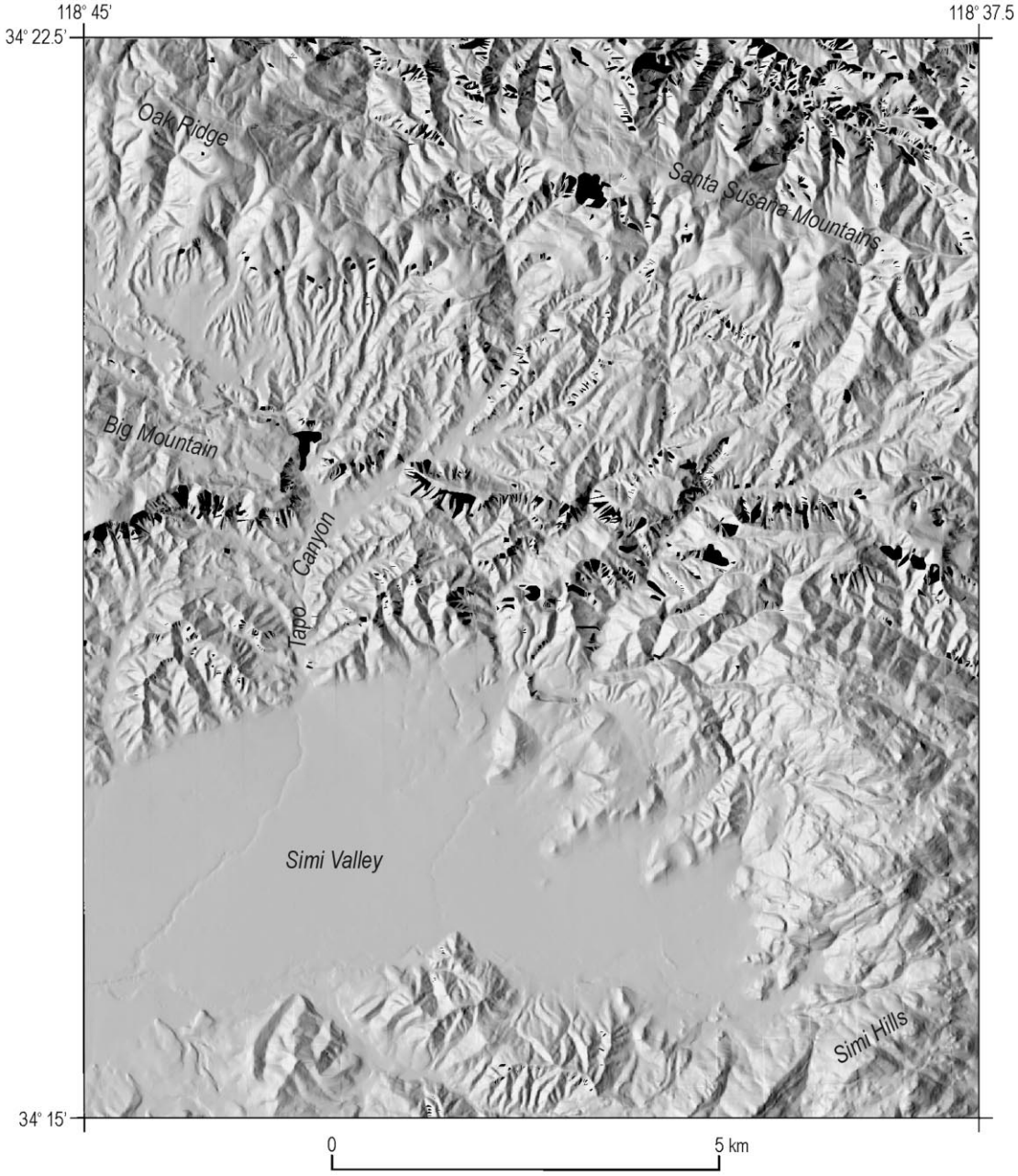

Fig. 2. Digital elevation model of the Santa Susana quadrangle; landslides triggered by the Northridge earthquake shown in black.

conglomerate and siltstone. The area between Big Mountain and Simi Valley, in the west–central part of the quadrangle, consists of the Oligocene and Eocene Sespe Formation, made up of sandstone, conglomerate, and claystone.

The Simi Hills, bounding the Simi Valley on the south and west, are composed of the oldest and strongest formations in the quadrangle. Principal formations include: (1) the Upper Cretaceous Chatsworth Formation, a well-

Table 1
Geologic units and lithologies (from Yerkes and Campbell, 1995) in the Santa Susana quadrangle

Geologic unit	Unit	Age	Lithologic description
Alluvium	Qal	Holocene	Alluvial deposits
	Qao	Holocene–Pleistocene	Older alluvial deposits
Landslide deposits	Qls	Holocene–Pleistocene	Landslide deposits
	Qls?	Holocene–Pleistocene	Likely landslide deposits
Pleistocene deposits	Qsw	Holocene–Pleistocene	Slope wash
	Qt	Pleistocene	Terrace deposits
	Qft	Pleistocene	Fan and terrace deposits undivided
Saugus Formation	Qs	Pleistocene	Sandstone, conglomerate, siltstone
	Qsm	Pleistocene	Sandstone and conglomerate
Pico Formation	QTp	Pleistocene–Pliocene	Sandy siltstone, sandstone, and pebbly sandstone
	QTpc	Pleistocene–Pliocene	Sandstone and conglomerate
	QTps	Pleistocene–Pliocene	Siltstone
Towsley Formation	Tw	Early Pliocene–Late Miocene	Fine- to coarse-grained sandstone
	Twc	Early Pliocene–Late Miocene	Chiefly sandstone
	Tws	Early Pliocene–Late Miocene	Chiefly siltstone or mudstone
Modelo Formation	Tm	Middle?–Late Miocene	Shale, silty to sandy, cherty, siliceous, diatomeceous, or clayey, interbedded sandstone
	Tm2	Middle?–Late Miocene	Siliceous shale and bedded chert
	Tm3	Middle?–Late Miocene	Diatomeceous to siliceous shale and chert
	Tm4	Middle?–Late Miocene	Siltstone with limestone concretions
	Tmd	Middle?–Late Miocene	Diatomeceous shale
Topanga Group	Tt	Middle Miocene	Sandstone
Sespe Formation	Ts	Oligocene–Late Eocene	Sandstone, conglomerate, and claystone
Llajas Formation	Tl	Early–Middle Eocene	Conglomerate, sandstone, and siltstone
	Tlc	Early–Middle Eocene	Pebble conglomerate and interbedded thin sandstone
Santa Susana Formation	Tss	Late Paleocene–Early Eocene	Mudrock, with subordinate sandstone and conglomerate
Simi Conglomerate	Tsc	Paleocene	Conglomerate, interbedded sandstone, minor mudrock
Chatsworth Formation	Kc	Upper Cretaceous	Sandstone, with interbeds of siltstone

cemented sandstone; (2) the locally well-cemented Simi Conglomerate of Paleocene age; (3) the Paleocene–Eocene Santa Susana Formation, consisting of mudstone with local sandstone interbeds; and (4) the Eocene Llajas Formation, consisting of sandstone, siltstone, and conglomerate.

We analyzed landslides in the Santa Susana quadrangle using digital data sets rasterized in 10 m cells. Topography was characterized using a digital elevation model (DEM) scanned from US Geological Survey contour plates from which 1:24,000 scale paper maps are produced. We produced a slope map by processing the DEM through a simple algorithm that calculates the maximum slope between each cell and its nearest neighboring cells. The DEM has the same limitations as the published contour maps, including underestimation of slope angles steeper than about 60–70° (Harp and Jibson, 1995, 1996). The geology of the Santa Susana quadrangle was taken from a digital map compiled at 1:24,000 scale by Yerkes and Campbell (1995, 1997). Landslides were rasterized from the digital inventory of triggered landslides (in vector form) compiled by Harp and Jibson (1995, 1996). Ground shaking intensities from the Northridge earthquake were interpolated from the roughly 200 strong-motion stations in the region using a simple kriging algorithm (Jibson et al., 1998; this volume).

5. Frequency and morphometry of triggered landslides in the Santa Susana quadrangle

5.1. Numbers and types of landslide

A total of 1562 seismically triggered landslides were mapped in the Santa Susana quadrangle. These landslides cover an area of about 3.4 km^2,

Geologic unit	Exposure area (sq.km)	Proportional exposure (percent)
Alluvium	35.1	22.1
Landslide deposits	11.4	7.1
Pleistocene deposits	5.7	3.6
Saugus Formation	15.2	9.5
Pico Formation	2.1	1.3
Towsley Formation	12.7	7.9
Modelo Formation	20.8	13
Topanga Group	0.2	0.1
Sespe Formation	11.3	7.1
Llajas Formation	8.8	5.6
Santa Susana Formation	10.4	6.5
Simi Conglomerate	5.2	3.3
Chatsworth Formation	20.6	12.9

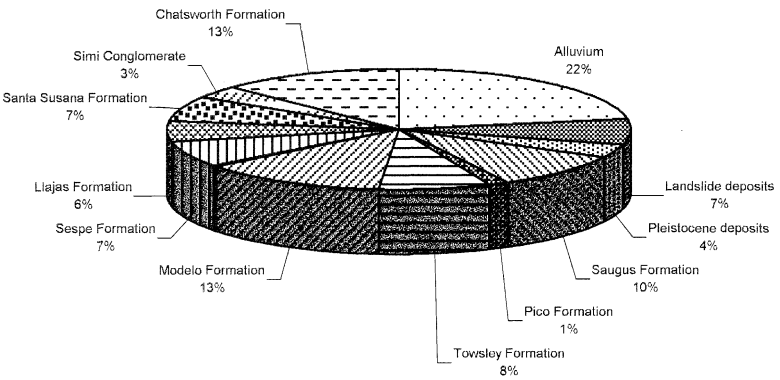

Fig. 3. Distribution of geologic units in the Santa Susana quadrangle.

which is more than 2% of the entire quadrangle. The landslides are primarily concentrated in two bands (Fig. 2). The largest concentration extends northwest–southeast through the Santa Susana Mountains. The maximum concentration of landslides in this area occurs in the northeast corner of the quadrangle in the Towsley Formation. Jibson et al. (1994b) pointed out that some local drainages within the Santa Susana Mountains had more than 75% of their slope areas denuded by landsliding triggered by strong shaking during the earthquake. The second band trends east–west across the central part of the Santa Susana quadrangle and includes the slopes along the northern border of the Simi Valley. Other landslides are scattered in various parts of the quadrangle, primarily in its northern half; very few slides occur along Oak Ridge or in the Simi Hills.

The large majority of the triggered landslides were shallow disrupted falls and slides in rock and soil. Most of these landslides were perhaps 1–2 m deep and thus occurred in the zone of weathered bedrock and colluvium.

To facilitate morphometric and statistical analyses on the landslides triggered by the earthquake, we separated the landslides in the Santa Susana quadrangle into two sample groups: single landslides and landslide complexes. A single landslide is an individual feature involving material that moved from a single, clearly defined source area;

single landslide boundaries are generally easy to identify both in the field and on aerial photos (Fig. 4). Landslide complexes, on the other hand, are areas where seismic shaking triggered multiple coalescing failures of surficial material, and it was not possible to outline the boundaries of each individual landslide (Fig. 5). The distinction between single landslides and landslide complexes does not imply any difference in landslide typology.

A total of 1502 single landslides covered 2.3 km^2. By contrast, only 60 landslide complexes occurred, but they covered about 1.0 km^2 (Table 2). Thus, landslide complexes account for only 4% of the total number of landslides, but

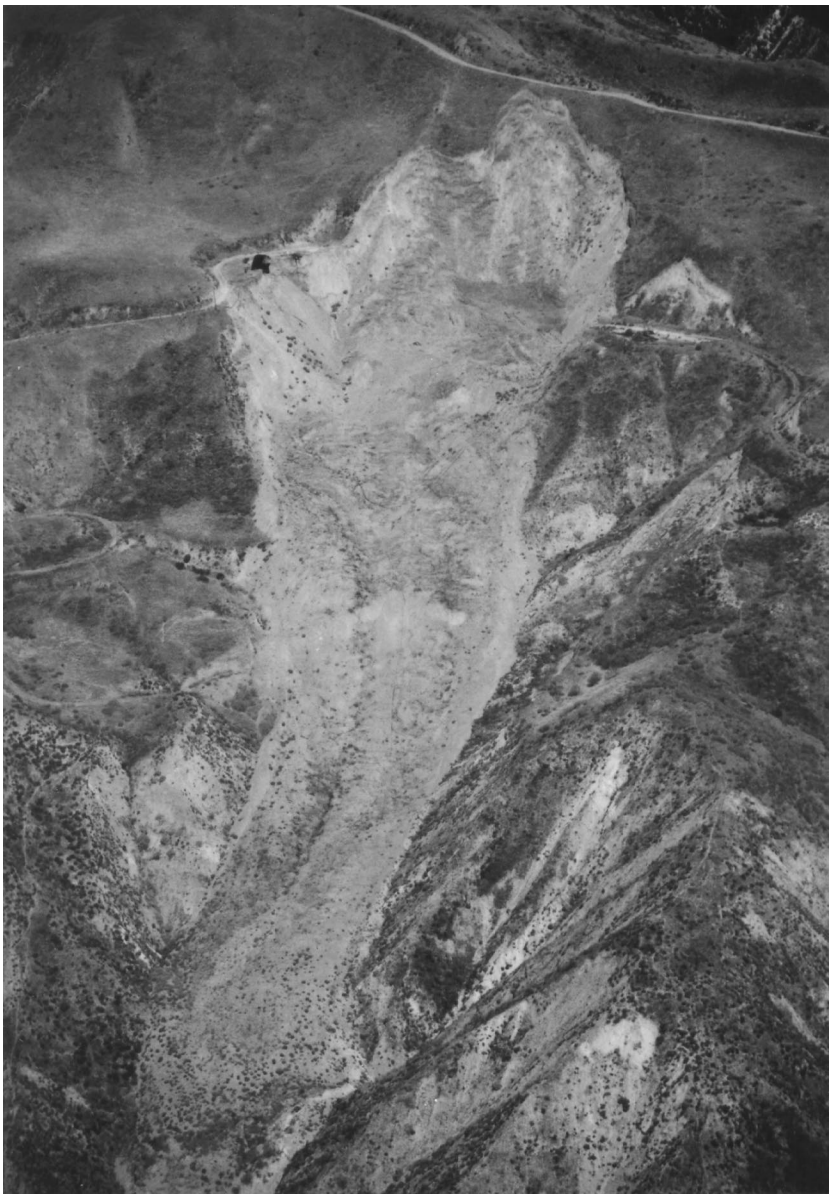

Fig. 4. Example of single landslide: oblique aerial view of the Ramona Oil Field earth slide/flow.

Fig. 5. Landslide complexes on a slope in the Santa Susana Mountains.

these complexes account for 31% of the area affected by landslides.

5.2. Landslide morphometry

Simple morphometric parameters — including area, length, width, aspect ratio, and slope angle — were computed for both single landslides and landslide complexes using a 10 m DEM in Arc/Info (Table 2). Landslide features and dimensions are described following the definitions of the IAEG Commission on Landslides (1990). Single landslide areas ranged from 23 m^2 to more than 25,000 m^2 and averaged 1520 m^2. Landslide complexes averaged more than 10 times larger, at more than 17,000 m^2, and ranged in area from almost 2500 m^2 to more than 100,000 m^2.

Total length (the minimum distance from the crown of a landslide to its tip) was computed along the direction of landslide movement. Width was measured perpendicular to total length in the area of maximum landslide breadth. Lengths of single slides ranged from 9 to more than 350 m and averaged about 70 m; lengths of landslide complexes averaged more than twice as great at 186 m. Single landslide widths ranged from 4 to almost 200 m and averaged 26 m. Landslide complexes, which commonly extended along entire ridge lengths (as is apparent in Fig. 5), had average widths of more than 150 m and were as wide as 543 m.

The shape of a landslide can be described by its aspect (length/width) ratio. Comparable values of length and width, yielding aspect ratios close to 1, are typical of rotational slides, and, to a lesser extent, translational slides and soil slips. When the length is much greater than the width, the ratio increases, indicating elongated shapes typical of

Table 2
Frequency and morphometric parameters of landslides triggered by the Northridge earthquake in the Santa Susana quadrangle

		Single landslides	Landslide complexes
Frequency		1502	60
Area (m^2)	Total	2,343,100	1,032,400
	Minimum	23	2471
	Maximum	25,257	106,765
	Mean	1520	17,324
	Standard deviation	2061	19,121
Length (m)	Minimum	9	50
	Maximum	367	435
	Mean	69	186
	Standard deviation	47	87
Width (m)	Minimum	4	49
	Maximum	195	543
	Mean	26	154
	Standard deviation	21	115
Mean aspect ratio		2.6	1.2
Slope (°)	Mean	36	38
	Range of mean	8–60	11–55
	Maximum	12–70	27–71

flow-type landslides as well as disrupted slides having long to very long runout distances.

Aspect ratios in Table 2 clearly show the elongated shape of the great majority of single landslides, which have a mean ratio of 2.6. This elongation resulted, in general, from moderately long runout distances down steep slopes below landslide source areas. Landslide complexes, on the other hand, have mean ratios of 1.2, indicating very little elongation. Although their runout distances averaged longer than those for single landslides, most of the complex landslides extended for large distances along ridge lines, which yielded aspect ratios near 1.

Maximum and mean slope angle were computed in landslide source areas (Table 2). For both single and complex landslides, mean slopes in landslide source areas were about 35–40°. Ranges of slope angles, however, were quite large: single landslides ranged from 8 to 60°, and landslide complexes ranged from 11 to 55°. Maximum slopes in source areas vary from 12 to 70° for single landslides, and from about 27 to 71° for landslide complexes.

Landslide azimuth indicates the main direction of movement of the landslide. Azimuth was measured from north in a clockwise direction following the total length of the landslide; in cases of a landslide having one or more changes of direction in its path, azimuth was measured in its upper part. Fig. 6 shows, respectively, the distribution of landslide azimuths for single landslide and for landslide complexes, expressed as a percentage. For single landslides [Fig. 6(A)], azimuth directions are generally clustered in the southern sectors, from SE to SW, while a very small number of landslides moved on slopes exposed to the northern sectors. Movement in a southward direction prevails for the landslide complexes, as well [Fig. 6(B)], with a peak, corresponding to a value greater than 10%, visible between 160 and 170°; however, the overall distribution of azimuths for landslide complexes, with several secondary peaks, is more random than for single landslides.

As noted above, the most prominent physiographic feature in the Santa Susana quadrangle is the E–W and ESE–WNW orientation of its elongate mountains and valleys. Such a feature clearly affects the distribution of the landslide azimuths, as shown by their concentration in the southern sectors. On the other hand, the very small number of azimuths in the northern sector is worth noting. One possible explanation for this is that geologic units in this area generally dip southward; thus, the predominance of landslides on south-facing slopes could indicate that dip slopes are far more susceptible to seismic failure than reverse-dip slopes. Another possibility is that south-facing slopes are more deeply weathered than north-facing slopes on account of having more direct exposure to the sun.

6. Analysis of landslide distribution

6.1. Factors affecting landslide distribution in the Santa Susana quadrangle

In general, distributions of seismically triggered landslides are most strongly influenced by shaking intensity, slope geometry, and geology. The sections that follow examine each of these factors

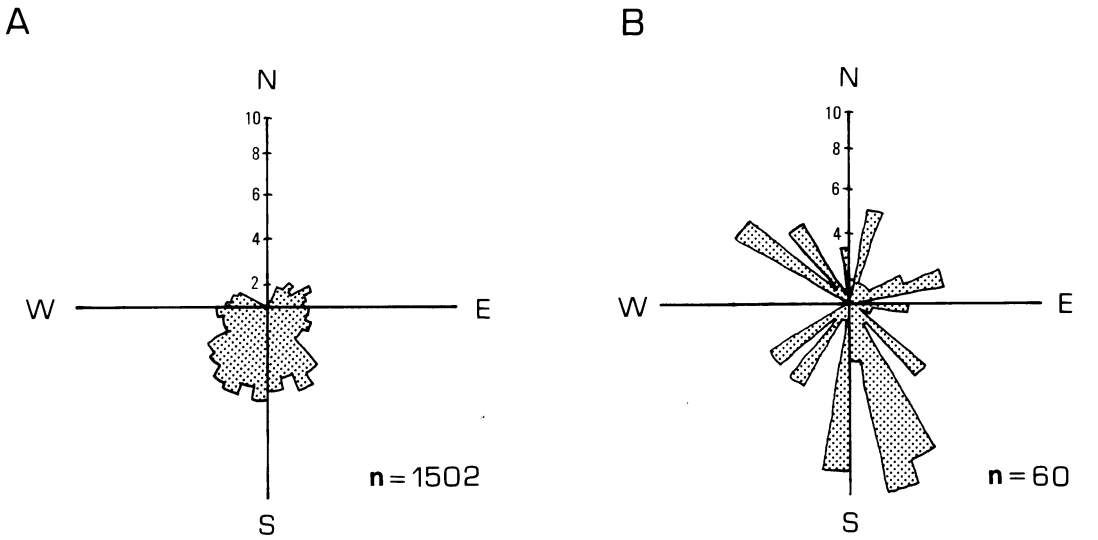

Fig. 6. Rose diagram of azimuth for (A) single landslides and (B) landslide complexes. Data expressed as a percentage.

and their influence on landslide distribution in the Santa Susana quadrangle.

Other factors can also affect the susceptibility of slopes to seismic triggering; some of these include groundwater conditions, vegetation, and human alteration of slopes. In the case of the Northridge earthquake, however, none of these factors is likely to have affected the distribution of triggered landslides. Virtually no rain had fallen for several months, and the fractured, primarily coarse-grained surficial slope materials were very dry. Vegetation throughout the area consists primarily of mixed grasses and shallow-rooted chaparral that would have little effect on slope stability. The steeply sloping areas in this quadrangle are virtually undeveloped, and very few of the landslides occurred near the sparse roads that exist in the steeply sloping areas; therefore, human influences on the landslide distribution appear negligible.

6.2. Effects of seismic shaking on landslide distribution

Most of the Santa Susana quadrangle was saturated with very high levels of ground shaking during the Northridge earthquake. Epicentral distances to the nearest and farthest corners of the quadrangle were 9 and 27 km, respectively, but almost half of the quadrangle was underlain by the projected seismogenic fault-rupture surface and thus was on the hanging wall above the thrust fault, where shaking tends to be enhanced. We measure shaking intensity in terms of Arias (1970) intensity, a single numerical measure of the shaking intensity of a strong-motion record determined by integrating the squared acceleration values; Arias intensity thus has units of velocity (Jibson, 1993). A regional contour map (Jibson et al., 1998; this volume) interpolated from about 200 strong-motion stations indicates a range of Arias intensities within the quadrangle from the Northridge earthquake of 1.14 to 3.92 m/s, which corresponds roughly to a range of peak ground accelerations (PGA) of 0.35 to 1.00 g. The mean Arias intensity in the quadrangle was 2.43 m/s, corresponding to a PGA of about 0.75 g. This is a very high level of ground shaking.

Over broad regions, triggering of landslides correlates strongly with the distribution of ground shaking intensities (Harp and Wilson, 1995). Within the limited area of the Santa Susana quadrangle, we compared landslide and shaking intensity distributions to detect any correlation. To do

this, we sorted all of the 10 m grid cells in the quadrangle into bins having Arias intensity widths of 0.25 m/s; thus, we created 12 bins spanning the observed Arias intensity range of 1–4 m/s. For each bin, we calculated the proportion of cells in that bin that were in landslide source areas. Fig. 7 shows the resulting plot. Increasing Arias intensity shows no positive or consistent correlation with increasing landslide occurrence; if anything, there is a slight negative correlation. This strongly suggests that the entire quadrangle experienced ground shaking above the intensity required to trigger slope failure and that factors other than ground shaking (such as geology and slope geometry) controlled the distribution of landslides in this area near the earthquake source. Also, topographic amplification and focusing of ground shaking in the steep terrain of the quadrangle may have exerted more influence on the ground shaking distribution than the simple attenuation modeled by the regional shaking data.

Fig. 8 plots the mean Arias shaking intensity ($\pm$ one standard deviation) in the Northridge earthquake for each of the geologic units in the quadrangle (Table 3). Bars for most units overlap within a narrow band between 1.5 and 3.0 m/s, which further indicates that for the purposes of analyzing the landslide distribution, ground shaking can be considered to be fairly uniform between geologic units throughout the quadrangle. Interestingly, the two units that experienced the most intense ground shaking, Qsw and Kc, had the lowest incidence of landsliding during the earthquake.

6.3. Landslide distribution by slope angle

Slope angle exerts a significant influence on landslide susceptibility: all things being equal, steeper slopes are more susceptible to failure than flatter slopes. We analyzed the influence of slope angle on landslide distribution very simply by calculating slope areas and numbers of landslides in 5° bands of slope angle. Fig. 9(A) shows the distribution of slope angles in the quadrangle in terms of area. Slopes are fairly evenly distributed around a central value of about 25°; areas of steeper slopes fall off abruptly above about 30°.

Fig. 9(B) shows the distribution of landslides with respect to slope angle, and the population is strongly concentrated on slopes in the 30–45° range, with more than three-quarters of all the landslides falling in this range. Thus, as we intuitively expect, the landslide population is skewed significantly toward steeper slopes relative to the population of slopes in general.

Fig. 9(C) shows landslide density with respect to slope angle; the figure was produced simply by dividing the number of landslides [Fig. 9(B)] by

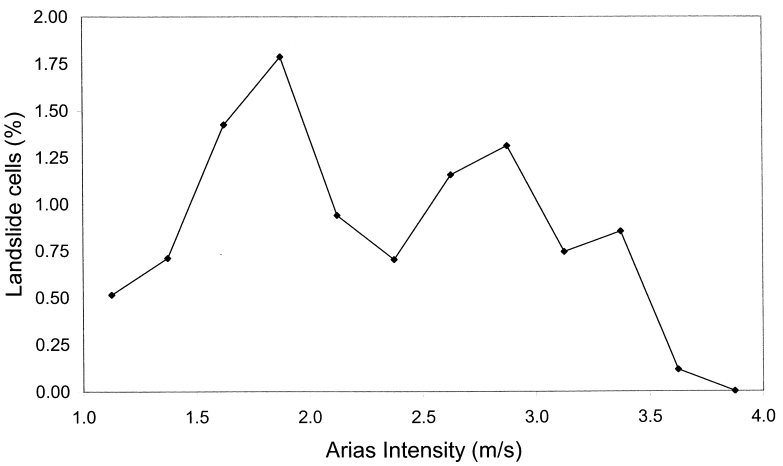

Fig. 7. Landslide occurrence as a function of Arias shaking intensity.

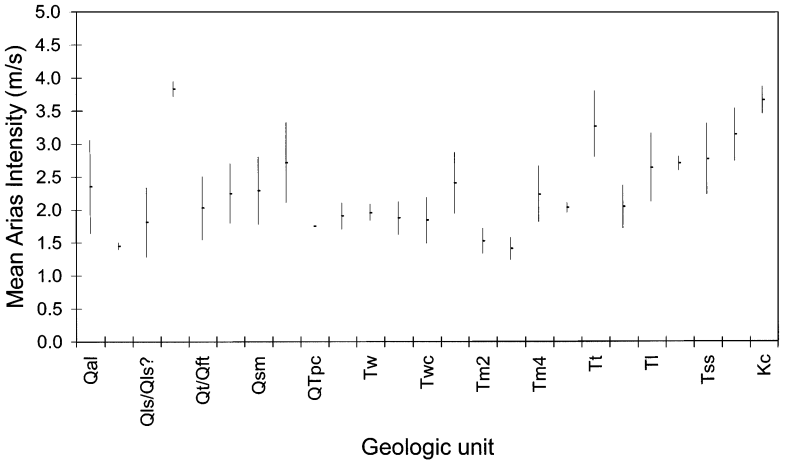

Fig. 8. Mean Arias intensity (±one standard deviation) from the Northridge earthquake in geologic units in the Santa Susana quadrangle.

the slope area [Fig. 9(A)]. Landslide density is skewed even farther toward the steep slopes, with the maximum values — about 100 landslides/km^2 — in the 40–50° range. Thus, although there are relatively few slopes in this steep range, they produced very high densities of landslides.

Intuitively, one might expect the landslide density distribution [Fig. 9(C)] to continue to increase with increasing slope angle rather than decreasing in the highest slope ranges (50–60°). The most probable explanation for the decrease at the highest slope angles is that the steepest slopes in the area form in the strongest units, which can support such steep slopes, or in locally well-cemented beds of otherwise weaker units.

6.4. Landslide distribution by geologic unit

Fig. 10 and Table 3 show landslide occurrence by geologic unit. The greatest areal extent of landslides (more than 1 km^2) was in the Towsley Formation. The Modelo, Sespe, Llajas, and Pico Formations, respectively, had the next highest areas affected by landslides. Alluvium, Pleistocene deposits, the Topanga Group, and the Chatsworth Formation are the only geologic units whose landslide areas do not exceed 10,000 m^2.

Some formations are divided into informal units, and considerable variability in landslide occurrence exists between units. The fine-grained unit of the Towsley Formation (Tws) is by far the most affected by landsliding, with a total landslide area greater than 625,000 m^2. Shale and interbedded sandstone of the Modelo Formation (Tm), sandstone of the Towsley Formation (Twc), conglomerate, sandstone, and siltstone of the Llajas Formation (Tl) all have landslide areas greater than 300,000 m^2 (Table 3).

Table 3 also lists numbers of landslides in the geologic units. The total number of landslides from this table is much greater than the 1502 single landslides and 60 landslide complexes reported in Table 2 because landslides involving more than one geologic unit were counted in both affected units. The Towsley Formation, with 611 landslides, has the greatest number of landslides. The Modelo (392), Sespe (242), Llajas (212), Saugus (173), and Pico (146) Formations also have relatively high landslide occurrences.

Table 3 compares areas of single landslides and landslide complexes for each geologic unit. The Towsley, Modelo, Sespe, and Llajas Formations had the largest areas of both single landslides and landslide complexes.

The geologic map includes Quaternary landslides (Qls); these are primarily large, deep slide masses that did not reactivate during the earthquake. Very few of the triggered landslides

Table 3
Exposure areas, shaking intensities, and landslide areas and frequencies for geologic units

Geologic unit	Mean Arias intensity (m/s)	Exposure area (m^2)	Landslide area (m^2)			Landslide source areas (m^2)	Number of landslides	Susceptibility index (%)	Frequency index (ls/km^2)
			Single	Complexes	Total				
Alluvium	2.28	35,133,900	30,400	22,500	52,900	9000	32	0.03	0.9
Qal	2.36	33,878,300			52,900	9000	32	0.03	0.9
Qao	1.45	1,255,600			0	0	0	0	0
Landslide deposits	1.82	11,388,300	65,000	41,500	106,500	57,600	80	0.51	7.0
Pleistocene deposits	2.04	5,694,100	7500	0	7500	2000	15	0.04	2.6
Qsw	3.84	37,400			0	0	0	0	0
Qft/Qt	2.03	5,656,700			7500	2000	15	0.04	2.7
Saugus Formation	2.27	15,191,800	151,900	45,700	197,600	144,400	173	0.95	11.4
Qs	2.25	7,980,400			91,700	49,400	86	0.62	10.8
Qsm	2.29	7,211,400			105,900	65,000	87	0.90	12.1
Pico Formation	2.45	2,064,700	156,800	97,100	253,900	155,000	146	7.51	70.7
QTp	2.72	1,379,100			127,500	82,300	82	5.97	59.5
QTpc	1.75	29,800			6300	5100	5	17.11	167.8
QTps	1.91	655,800			120,100	67,600	59	10.31	90.0
Towsley Formation	1.87	12,659,800	868,900	262,500	1,131,400	532,500	611	4.21	48.3
Tw	1.95	644,500			58,800	29,800	40	4.62	62.1
Twc	1.85	6,810,400			446,900	209,700	259	3.08	38.0
Tws	1.88	5,204,900			625,700	293,000	312	5.63	59.9
Modelo Formation	2.10	20,794,200	407,500	277,000	684,500	340,900	392	1.64	18.9
Tm	2.41	7,572,300			422,400	207,900	252	2.75	33.3
Tm2	1.53	3,975,300			39,500	20,200	24	0.51	6.0
Tm3	1.42	1,690,700			1300	600	2	0.04	1.2
Tm4	2.24	7,096,100			199,800	104,200	98	1.47	13.8
Tmd	2.04	459,800			21,500	8000	16	1.74	34.8
Topanga Group	3.27	241,100	4800	1400	6200	2800	19	1.16	78.8
Sespe Formation	2.05	11,284,600	273,700	200,200	473,900	209,100	242	1.85	21.4
Llajas Formation	2.64	8,850,700	245,600	109,000	354,600	152,000	212	1.72	24.0
Tl	2.64	8,734,500			329,600	144,000	197	1.65	22.6
Tlc	2.71	116,200			25,000	8000	15	6.88	129.1
Santa Susana Formation	2.77	10,437,400	52,200	3700	55,900	26,600	58	0.25	5.6
Simi Conglomerate	3.14	5,188,900	47,800	0	47,800	19,800	67	0.38	12.9
Chatsworth Formation	3.66	20,567,900	2800	0	2800	1200	6	0.01	0.3

involved reactivation of pre-existing landslide masses. However, many of the shallow, disrupted slides initiated on steep slopes that undoubtedly have produced landslides in the past. Mapped Quaternary landslides occupy 7.1% of the quadrangle, but only 3.3% of the landslides triggered by the Northridge earthquake occur in the mapped Quaternary landslides. Thus, far from having an increased susceptibility to landsliding, mapped Quaternary landslides produced new landslides at less than half the average rate of all the units in the quadrangle. This is probably because landslides mapped on the geologic map are large, deep, coherent masses that did not experience significant disruption during movement.

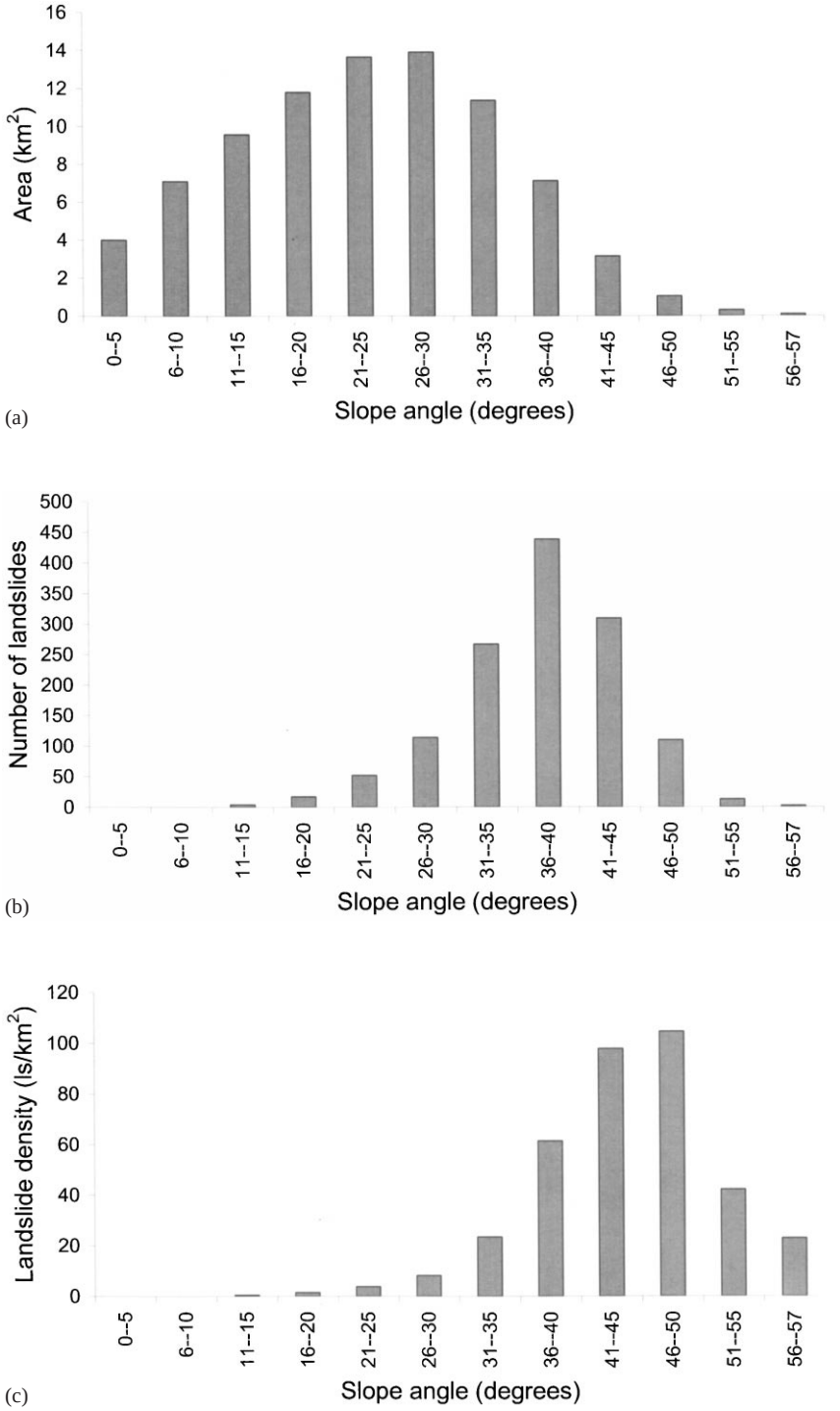

Fig. 9. (a) Distribution of slope angles by area in the Santa Susana quadrangle. (b) Distribution of landslides by slope angle. (c) Distribution of landslide density as a function of slope angle.

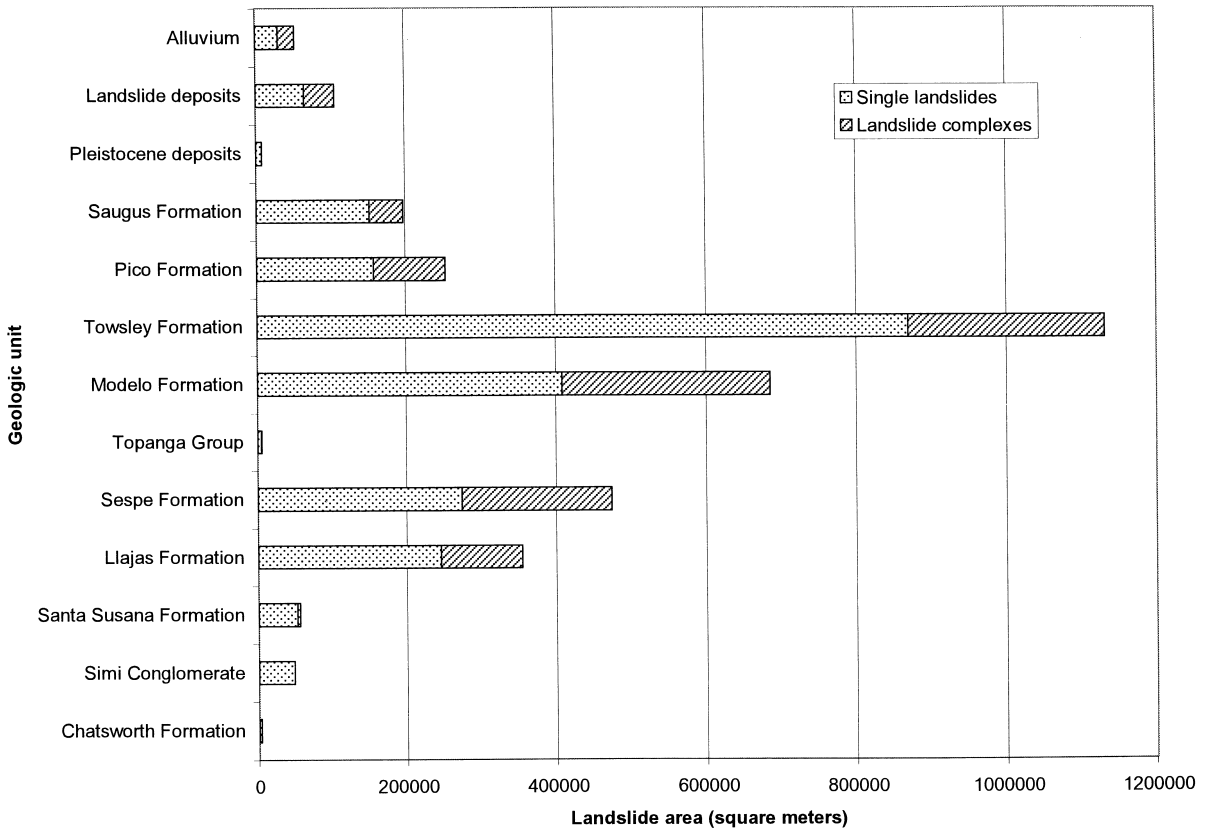

Fig. 10. Landslide areas of geologic units for single landslides and landslide complexes.

7. Seismic landslide susceptibility of geologic units

7.1. Landslide susceptibility index

The total area affected by landslides in a particular geologic unit depends, in part, on the aerial exposure of that unit within the study area. A measure of the susceptibility of each unit to seismic slope failure can be developed by simply dividing the area of landslide sources (defined as the upper half of a mapped landslide) within each unit by the total outcrop area of that unit (Table 3). This yields the percentage of the outcrop area that failed, which we term the susceptibility index. Fig. 11 and Table 3 show the susceptibility indices of geologic units.

The Pico (7.51%) and Towsley (4.21%) Formations have the highest susceptibility indices. The Sespe (1.85%), Llajas (1.72%), Modelo (1.64%), and Topanga (1.16%) Formations also have susceptibility indices greater than the average value (1.02%) for the entire quadrangle.

In regard to geologic units within formations, note the very high values of susceptibility index (Table 3) for the two units of the Pico Formation: sandstone and conglomerate (QTpc = 17.11%), and siltstone (QTps = 10.31%). The very small outcrop area of the QTpc unit of the Pico Formation makes drawing any conclusion about its susceptibility uncertain; on the other hand, the QTps unit of the Pico Formation does appear to have very high susceptibility in the study area.

The Chatsworth Formation (0.01), Alluvium (0.03), and Pleistocene deposits (0.04) had the lowest values of susceptibility index.

7.2. Landslide frequency index

A measure of the frequency of landsliding within a geologic unit can be determined by simply

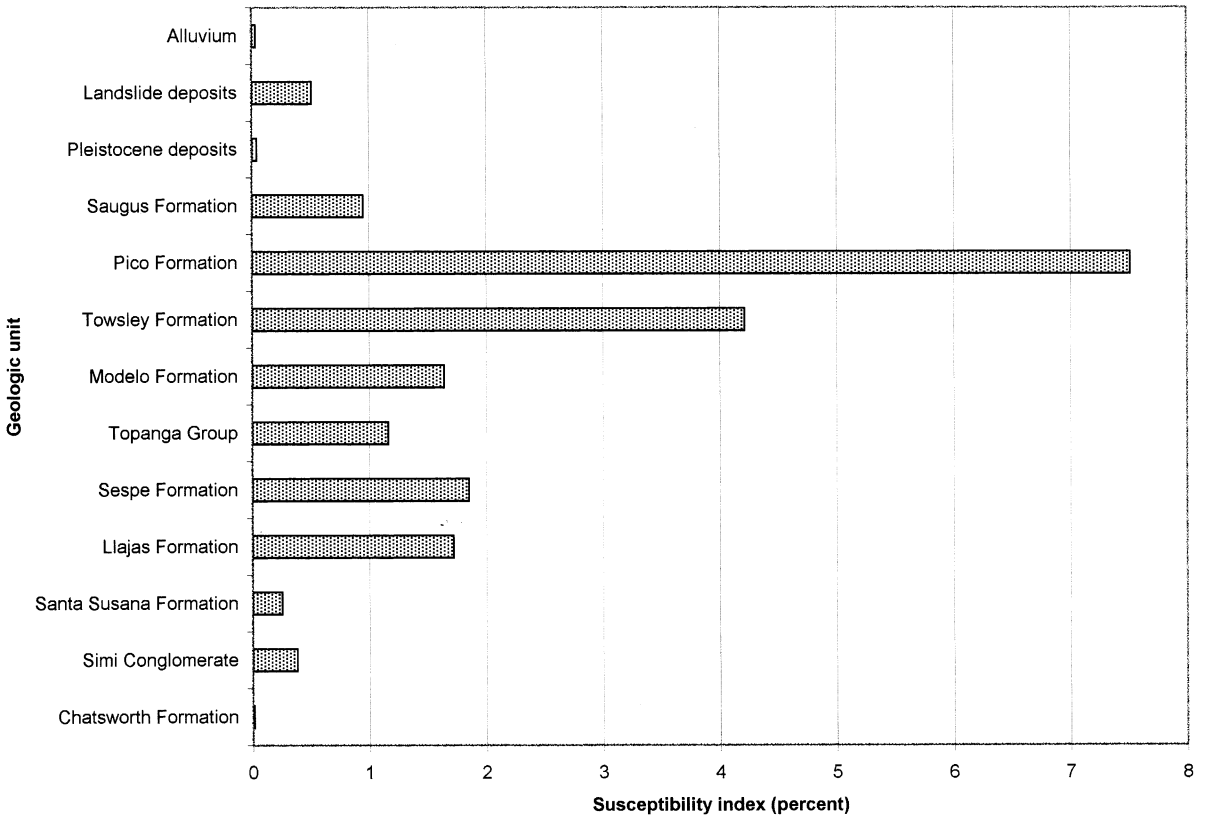

Fig. 11. Susceptibility index of geologic units.

dividing the number of landslides within a unit by the exposure area of that unit, which indicates the number of landslides per square kilometer (ls/km^2). A very broad range of landslide frequencies is apparent (Fig. 12, Table 3). The Topanga (78.8 ls/km^2), Pico (70.7 ls/km^2), and Towsley (48.3 ls/km^2) Formations have the highest frequency indices. The Llajas, Sespe, Modelo, and Saugus Formations and the Simi Conglomerate have moderately high frequencies ranging from 11 to 24 ls/km^2. The lowest frequency indices are in the Alluvium (0.9 ls/km^2) and the Chatsworth Formation (0.3 ls/km^2).

Values of frequency index for the geologic units within formations are generally similar to those for the corresponding entire formations, but a few exceptions are present. Very high frequency indices were observed in three geologic units: 167.8 ls/km^2 in the sandstone and conglomerate (QTpc) of the Pico Formation, 129.1 ls/km^2 in the conglomerate and interbedded sandstone (Tlc) of the Llajas Formation, and 90.0 ls/km^2 in the siltstone (QTps) of the Pico Formation. In each of these cases, the relatively small exposure areas of the units (see Table 3) may partly explain the extreme values; therefore, they should be checked with data from other quadrangles to verify their validity.

7.3. Evaluation of landslide susceptibility of geologic units

The two indices defined above provide an objective measure of relative seismic landslide susceptibility between geologic units. The susceptibility index measures the proportion of outcrop area that failed, and the frequency index measures the density of landslides, regardless of size. Inspection of Figs. 11

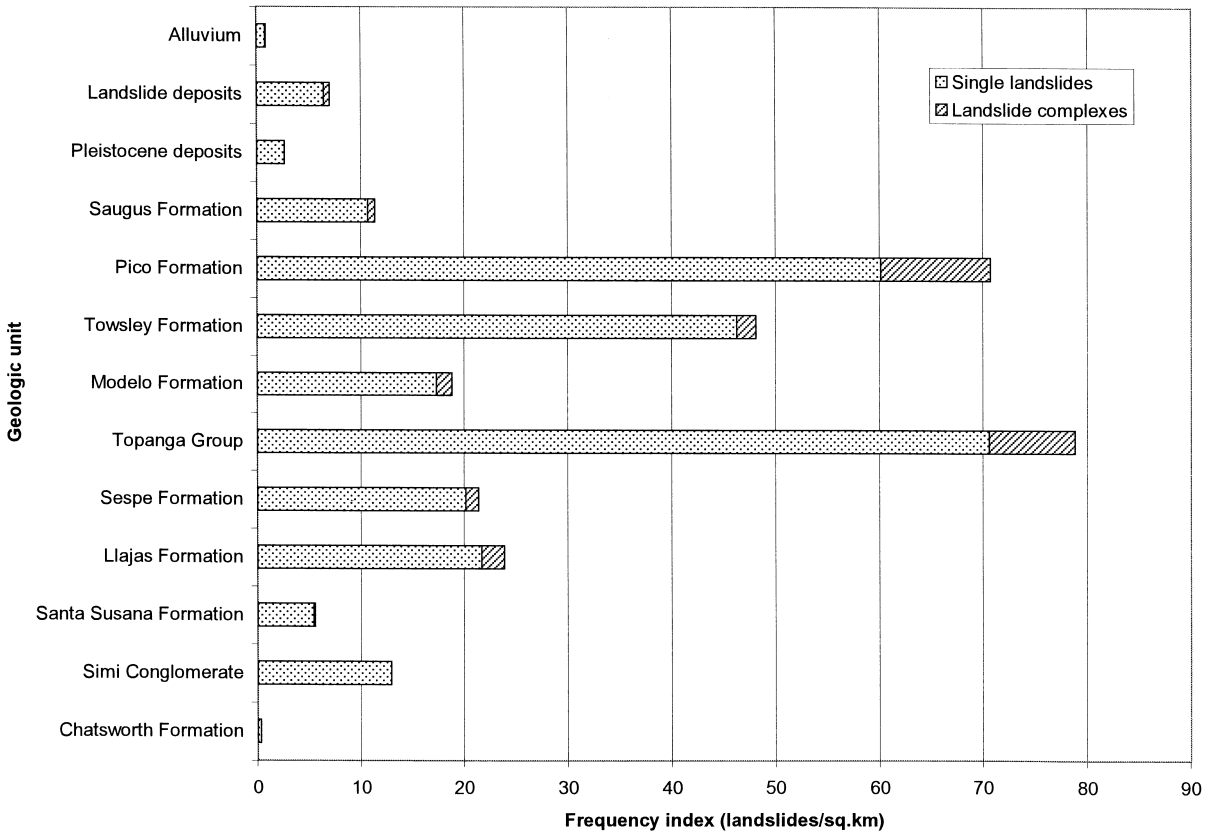

Fig. 12. Frequency index of geologic units for single landslides and landslide complexes.

and 12 and Table 3 indicates that, in most cases, the susceptibility rankings using the two methods yield similar results. One exception is the Topanga Group, which had the highest frequency index but a more moderate susceptibility index. This means that outcrops of the Topanga Group experienced large numbers of relatively small landslides.

Taking both indices into account, we propose the susceptibility ranking shown in Table 4 to evaluate the relative susceptibility to seismic triggering of landslides in the geologic units. Criteria for classification are as follows: susceptibility index greater than 2.5% or frequency index greater than 30 ls/km^2 is *very high susceptibility*; susceptibility index of 1.0–2.5% or frequency index of 10–30 ls/km^2 is *high susceptibility*; susceptibility index of 0.5–1.0% or frequency index of 3–10 ls/km^2 is *moderate susceptibility*; and susceptibility index less than 0.5% and frequency less than 3 ls/km^2 is *low susceptibility*.

Among the most susceptible units, the Pico and Towsley Formations are, by far, the most susceptible to seismically triggered failure. The Topanga Group did not affect a large proportion of its outcrop area but did produce a very large number of failures. Among bedrock units, the Chatsworth Formation is, by far, the least susceptible to seismic failure. These susceptibility rankings apply only to seismic triggering conditions; various geologic units may have different relative susceptibilities to failure in aseismic conditions.

8. Discussion

The data and analyses presented above provide a broad framework for anticipating characteristics

Table 4
Seismic landslide susceptibility rankings (listed in decreasing order of susceptibility) of geologic units

Geologic unit	Susceptibility index (%)	Frequency index (ls/km^2)	Seismic landslide susceptibility
Pico Formation	7.51	70.7	Very high susceptibility
Towsley Formation	4.21	48.3	
Topanga Group	1.16	78.8	
Sespe Formation	1.85	21.4	High susceptibility
Llajas Formation	1.72	24.0	
Modelo Formation	1.64	18.9	
Saugus Formation	0.95	11.4	
Simi Conglomerate	0.38	12.9	
Landslide deposits	0.51	7.0	Moderate susceptibility
Santa Susana Formation	0.25	5.6	
Pleistocene deposits	0.04	2.6	Low susceptibility
Alluvium	0.03	0.9	
Chatsworth Formation	0.01	0.3	

of landslide distributions in future southern California earthquakes. In short, we might reasonably expect future earthquakes to produce landslides having characteristics similar to those triggered by the Northridge earthquake. The morphometric data provide useful insights into the sizes and types of landslide that might be expected in future earthquakes. The susceptibility rankings indicate geologic units most likely to produce landslides (Table 4). The morphometric data also indicate the range of slope angles on which these landslides generally occur. Fig. 9 provides useful insights into the range of slope angles on which most seismically triggered landslides in this area occur: the majority of the triggered landslides occurred on slopes ranging from 30 to 45°. Although some landslides occurred on much gentler slopes, even as low as 12°, it is the slopes in the 30–45° range that should be the primary focus of concern in terms of where most landslides will occur. Steeper slopes in the 45–50° range, although much less numerous, should also be expected to produce high concentrations of landslides.

Although distributions of future seismically triggered landslides will be strongly affected by earthquake magnitude, location, and focal mechanism, our data provide a first approximation of what those landslide distributions will look like. More rigorous and detailed analyses of the data are required for more accurate forecasting of future seismic landslide hazards. Jibson et al. (1998; this volume) present a rigorous method for producing such maps of seismic landslide susceptibility and hazard in southern California.

9. Conclusions

Analysis of the landslides triggered by the Northridge earthquake provides valuable insights into the characteristics of seismically triggered landslides in southern California. Our susceptibility ranking of geologic units shows clear distinctions between the susceptibilities of various geologic units to failure during seismic shaking. The Pico and Towsley Formations have very high susceptibilities to seismically triggered failure, and several other units have high and moderate susceptibilities. Some geologic units within formations also showed particularly high susceptibilities: among them, conglomerate and interbedded sandstone (Tlc) of the Llajas Formation; sandstone and conglomerate (QTpc), and siltstone (QTps) of the Pico Formation. Landslide incidence in these units should be examined in other quadrangles to see if this extreme susceptibility is widespread.

Our results provide a useful characterization of seismically triggered landslides in southern California that can be used to anticipate the characteristics of landslides triggered by future earthquakes there.

Acknowledgements

Support for Mario Parise's research at the US Geological Survey facilities in Golden, CO was provided by a grant from the National Research Council of Italy. John Michael of the US Geological Survey assembled the GIS databases and extracted specific data sets from them.

References

Arias, A., 1970. A measure of earthquake intensity. In: Hansen, R.J. (Ed.), Seismic Design for Nuclear Power Plants. Massachusetts Institute of Technology Press, Cambridge, MA, pp. 438–483.

Cotecchia, V., 1986. Ground deformations and slope instability produced by the earthquake of 23 November, 1980 in Campania and Basilicata. Geol. Appl. Idrogeol. 21 (5), 31–100.

Harp, E.L., Jibson, R.W., 1995. Inventory of landslides triggered by the 1994 Northridge, California earthquake. US Geol. Surv. Open-File Rep. 95-213 17 pp.

Harp, E.L., Jibson, R.W., 1996. Landslides triggered by the 1994 Northridge, California earthquake. Bull. Seism. Soc. Am. 86, 1, part B, S319–S332.

Harp, E.L., Wilson, R.C., 1995. Shaking intensity thresholds for rock falls and slides: evidence from 1987 Whittier Narrows and Superstition Hills earthquake strong-motion records. Bull. Seism. Soc. Am. 85 (6), 1739–1757.

Hauksson, E., Jones, L.M., 1994. Seismology: the Northridge earthquake and its aftershocks. US Geol. Surv., Earthquakes and Volcanoes 25, 18–30.

IAEG Commission on Landslides, 1990. Suggested nomenclature for landslides. Bull. Int. Assoc. Eng. Geol. 41, 13–16.

Jibson, R.W., 1993. Predicting earthquake-induced landslide displacements using Newmark's sliding block analysis. Transport. Res. Rec. 1411, 9–17.

Jibson, R.W., Prentice, C.S., Borissoff, B.A., Rogozhin, E.A., Langer, C.J., 1994a. Some observations of landslides triggered by the 29 April, 1991 Racha earthquake, Republic of Georgia. Bull. Seism. Soc. Am. 84, 963–973.

Jibson, R.W., Harp, E.L., Keefer, D.K., Wilson, R.C., 1994b. Landslides triggered by the Northridge earthquake. US Geol. Surv., Earthquakes and Volcanoes 25, 31–41.

Jibson, R.W., Harp, E.L., Michael, J.A., 1998. A method for producing digital probabilistic seismic hazard maps: an example from the Los Angeles, California area. US Geol. Surv. Open-File Rep. 98-113 17 pp.

Keefer, D.K., 1984. Landslides caused by earthquakes. Geol. Soc. Am. Bull. 95, 406–421.

Kobayashi, Y., 1981. Causes of fatalities in recent earthquakes in Japan. J. Disaster Sci. 3, 15–22.

Plafker, G., Galloway, J.P. (Eds.), Lessons learned from the Loma Prieta, California earthquake of October 17, 1989. US Geol. Surv. Circ. 1045 1989.

Schuster, R.L., 1996. Socioeconomic significance of landslides. In: Turner, A.K., Schuster, R.L. (Eds.), Landslides. Investigation and Mitigation. Transportation Research Board, National Academy Press, Washington, DC, pp. 12–35.

Shen, Z.K., Ge, B.X., Jackson, D.D., Potter, D., Cline, M., Sung, L., 1996. Northridge earthquake rupture models based on the global positioning system measurements. Bull. Seism. Soc. Am. 86, 1, part B, S37–S48.

Stewart, J.P., Chang, S.W., Bray, J.D., Seed, R.B., Sitar, N., Riemer, M.F., 1995. A report on geotechnical aspects of the January 17, 1994 Northridge earthquake. Seism. Res. Lett. 66 (3), 7–19.

Stewart, J.P., Seed, R.B., Bray, J.D., 1996. Incidents of ground failure from the 1994 Northridge earthquake. Bull. Seism. Soc. Am. 86, 1, part B, S300–S318.

Teng, T., Aki, K. (Eds.), Special Issue on the Northridge, California earthquake of January 17, 1994. Bull. Seism. Soc. Am. 86, 1, part B, 1996. 361 pp.

US Geological Survey, 1994. Northridge, California earthquake of January 17, 1994. Earthquakes & Volcanoes 25, 1/2, 112 pp.

US Geological Survey, 1996. USGS response to an urban earthquake: Northridge '94. US Geol. Surv. Open-File Rep. 96-263 78 pp.

Wald, D.J., Heaton, T., Wald, L., 1994. Rupture analysis of the Northridge earthquake from modelling strong motion recordings. US Geol. Surv., Earthquakes and Volcanoes 25, 42–47.

Wald, D.J., Heaton, T., Hudnut, K.W., 1996. The slip history of the 1994 Northridge, California earthquake determined from strong-motion, teleseismic, GPS, and leveling data. Bull. Seism. Soc. Am. 86, 1, part B, 49–70.

Yerkes, R.F., Campbell, R.H., 1995. Preliminary geologic map of the Santa Susana quadrangle, Southern California. US Geol. Surv. Open-File Rep. 95-829 12 pp.

Yerkes, R.F., Campbell, R.H., 1997. Preliminary geologic map of the Santa Susana quadrangle, Southern California: a digital database. US Geol. Surv. Open-File Rep. 97-258 (258) 12 pp.